Tuning the porosity of zinc oxide electrodes: from dense to nanopillar films

2015 Mater. Res. Express 2 075006

(http://iopscience.iop.org/2053-1591/2/7/075006)

Materials Research Express

PAPER

Tuning the porosity of zinc oxide electrodes: from dense to nanopillar films

RECEIVED
24 February 2015

REVISED
21 May 2015

ACCEPTED FOR PUBLICATION
3 June 2015

PUBLISHED
13 July 2015

Lorenzo Fanni[1], **Benoît Delaup**[1], **Bjoern Niesen**[1], **Yonat Milstein**[2], **Dubi Shachal**[2], **Monica Morales-Masis**[1], **Sylvain Nicolay**[3] **and Christophe Ballif**[1,3]

[1] Ecole Polytechnique Fédérale de Lausanne (EPFL), Institute of Microengineering (IMT), Photovoltaics and Thin-Film Electronics Laboratory, rue de la Maladière 71B, Neuchâtel CH-2000, Switzerland
[2] B-nano ltd, 2 Weisgal Rd. Rehovot 76326, Israel
[3] CSEM, PV-center, rue Jacques-Droz 1, Neuchâtel CH-2002, Switzerland

E-mail: lorenzo.fanni@epfl.ch

Keywords: nanopillar, zinc oxide, porosity, Kanaya Okayama

Abstract

Thin films with tunable porosity are of high interest in applications such as gas sensing and antireflective coatings. We report a facile and scalable method to fabricate ZnO electrodes with tuneable porosity. By adjusting the substrate temperature and ratio of precursor gasses during low-pressure chemical vapor deposition we can accurately tune the porosity of ZnO films, from 0 up to 24%. The porosity change of the films from dense layer to separated nanopillars results in an effective refractive index reduction from 1.9 to 1.65 at 550 nm, as determined by optical and x-ray spectroscopy. The low-refractive-index ZnO films are incorporated into amorphous silicon solar cells demonstrating reflection losses reduction down to 4% in the visible wavelengths range.

1. Introduction

Porous transparent conductive oxides are of interest for a wide range of applications, such as gas sensing [1–3], scaffolds for solar cells [4–6], and antireflective coatings [7, 8]. A common approach to estimate the properties of porous layers is to use the effective-medium theory, which predicts that the refractive index n of a thin film decreases as its void fraction increases [9, 10]. Indeed, for films with voids it is necessary to define an *effective* refractive index (n_{eff}) whose value is between that of air and that of the bulk material. By altering the compactness of the film and therefore its void density, the material refractive index can be tuned between these two extremes.

Here, we present the fabrication of zinc oxide (ZnO) electrodes with tunable density, ranging from dense layers to well-separated nanopillar structures. The ZnO films are deposited by low-pressure metal-organic chemical vapor deposition (LP-MOCVD), a technique that has been used since the end of the 1980s to produce transparent electrodes for thin-film solar cells [11]. Compared to other deposition techniques typically used for oxides (e.g. magnetron sputtering and solution processing), advantages of LP-MOCVD include the readily tunable microstructure and doping of the films [12, 14]. Here, we show that by adjusting the ratio of the precursor gases and the substrate temperature, the microstructure of the ZnO films can be tuned from dense to highly porous, without the use of complex processes [15, 16] and post-deposition treatments [17]. We optimize the porous films in order to minimize n_{eff}. We assess the film void fraction by means of energy-dispersive x-ray spectroscopy (EDX), and show that the results correlate well with the n_{eff} value obtained from optical measurements using transfer-matrix calculations. The facility of switching from dense to nanopillar film within the same deposition process as well as its application as an antireflective electrode is demonstrated by application in hydrogenated amorphous silicon (a-Si:H) solar cells. In this device the dense ZnO film is used as front electrode, providing electrical conductivity, and the nanopillar layer is applied on top of the the dense film reducing the reflectivity.

2. Experimental

2.1. Sample fabrication

For optical and morphological characterization, ZnO layers were deposited by LP-MOCVD on 0.5 mm thick AF32 Schott glass substrates. Diethylzinc (DEZ) and water vapor (H_2O) were used as precursors for zinc and oxygen, respectively. Non-intentionally doped (nid) films were obtained from DEZ and H_2O only, while doped films were obtained by adding B_2H_6 in the gas phase as precursor of boron (acting as donor in ZnO). All the precursor gases were injected into the chamber by simple precursor evaporation without a carrier gas. Dense films were obtained with a H_2O/DEZ flow ratio of 1 at a substrate temperature of 160 °C [12, 18]. For the nanopillar ZnO films, the substrate temperature was increased to 220 °C and the H_2O/DEZ flow ratio to 4. During deposition, the total pressure in the chamber was kept at 35 Pa. The thickness of the films varied between 0.65 and 1.2 μm. a-Si:H layers were deposited in the n–i–p configuration by plasma-enhanced chemical vapor deposition [19] while the front electrode was made of either the dense or dense/nanopillar film stacks as showed below (cfr. figure 5).

2.2. Characterization methods

The total transmittance and total reflectance of the films were measured in the 320–1200 nm spectral range using a spectrophotometer equipped with an integrating sphere. Due to the high surface area and roughness of the porous films it was not possible to perform ellipsometric measurements to assess n_{eff}; rather n_{eff} was derived from transmittance and reflectance curves using a software based on the transfer-matrix method (RefDex, developed at Helmholtz-Zentrum Berlin) [20]. The surface morphologies and cross sections of the films were analyzed by scanning electron microscopy (SEM, $V_{\text{ac}} = 5$ kV). The film density was derived from EDX measurements performed by the company B-nano [21]. The film sheet resistance (R_{sh}) was evaluated by four-point probe measurement.

3. Results and discussion

3.1. From dense to well-separated nanopillar films

Typical high-quality LP-MOCVD ZnO electrodes are deposited at a substrate temperature of 160 °C and a H_2O/DEZ ratio of 1 [12, 18]. These conditions provide the best trade-off between transparency and conductivity for application in solar cells. In addition, these films are dense and characterized by V-shaped grains having a preferential orientation along the *a*-axis of the wurtzite unit cell ('dense' in figure 1) [12, 18].

The film surface is rough due to pyramid-like features that provide high diffuse transmission, resulting in the typical hazy appearance of this material. Increasing the temperature during deposition leads to increased competition between crystalline orientations, such that the growth rates along different orientations become similar. Therefore the film structure becomes more disordered ('flaked' in figure 1) and without preferential orientation [22, 23]. In this case, the layer is characterized by flakes expanding in different directions and creating voids in the film. By further increasing the H_2O/DEZ ratio from 1 to 4, the deposition rate decreases. This is because at high temperatures the film growth is limited by the DEZ vapor concentration in the gas phase [12, 24]. The resulting structure is composed of separated nanopillars with an elongated section; the long side measures around 100 nm, and the short side measures around 30 nm ('nanopillars' in figure 1).

The change in film structure from dense to nanopillars leads to an increase in void fraction, inhibiting the lateral carrier transport (see section 3.3) but also increasing transmittance and simultaneously reducing reflectance, as shown in figure 2(a). The absorption of the different films is therefore similar. Noteworthy, n_{eff} derived from transmittance and reflectance at 550 nm decreases from $n_{\text{eff}} = 1.9$ for the dense film to $n_{\text{eff}} = 1.65$ for the nanopillar film. This change in effective refractive index can be explained by the effective-medium theory, which links the void fraction with the film's optical properties.

3.2. Assessing film density and its influence on effective refractive index

The effective-medium theory is used to estimate the optical properties of an inhomogeneous material by combining the properties of the constituent materials weighted by their volume fractions [25]. To derive optical properties in a mixed film, many models exist, each of which is most accurate only for distinct conditions [26–28]. Here, we calculate n_{eff} of the nanopillar films by assuming that they are composed of a mixture of dense ZnO with refractive index n_{ZnO}, and air ($n = 1$), using the Maxwell-Garnett equation [26]:

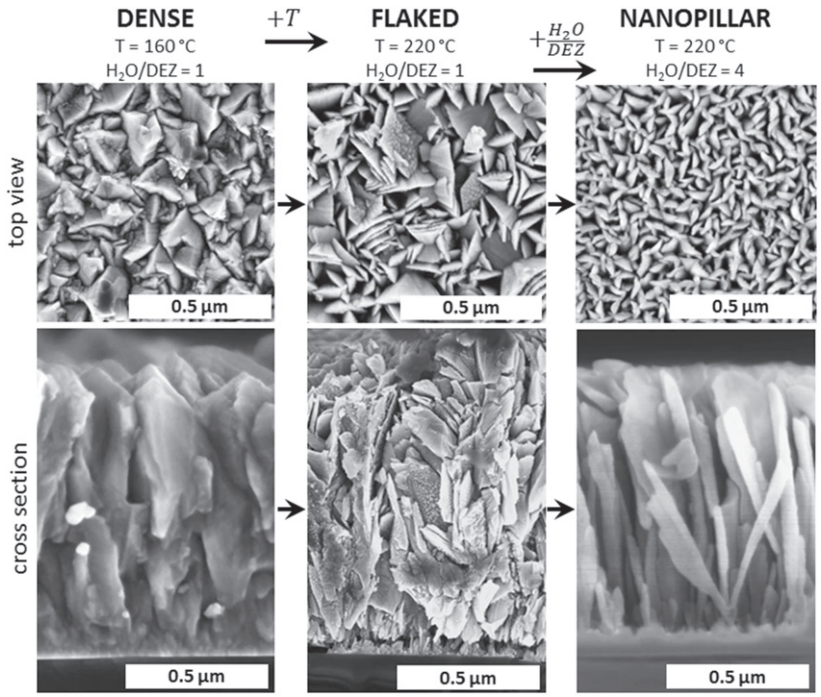

Figure 1. SEM images showing structural variations due to an increase in temperature and a subsequent increase in the H_2O/DEZ ratio.

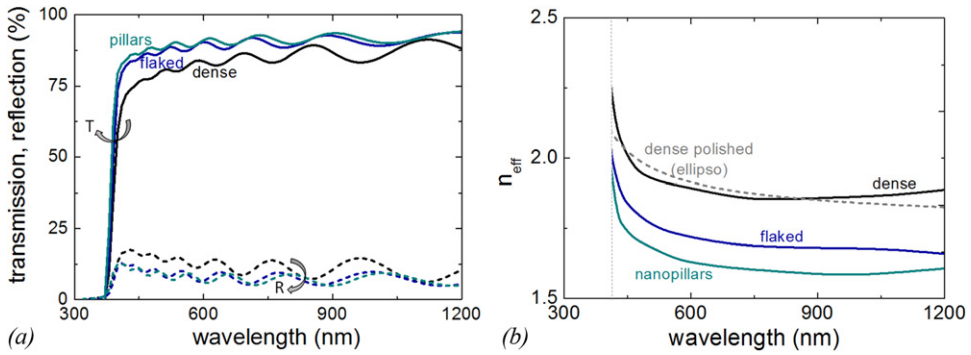

Figure 2. (a) Optical transmittance and reflectance of 1 μm thick dense, flaked, and nanopillar films. (b) Effective refractive index (n_{eff}) of 1 μm thick dense, flaked and nanopillar films. The curves are derived from the transmittance and reflectance spectra shown in figure 2(a). The refractive index of a polished dense film, measured with ellipsometry, is shown as a comparison; notice that below 400 nm the strong decrease in transmission prevents estimation of n_{eff} from spectrophotometry.

$$n_{\text{eff}} = n_{\text{ZnO}} \frac{2 \cdot \left(1 - \nu_{\text{f}}\right) \cdot n_{\text{ZnO}} + \left(1 + 2\nu_{\text{f}}\right)}{\left(2 + \nu_{\text{f}}\right) \cdot n_{\text{ZnO}} + \left(1 - \nu_{\text{f}}\right)} \quad (1)$$

with ν_{f} being the void fraction, and n_{ZnO} derived from spectroscopic ellipsometry measurements shown in figure 2(b). The refractive index obtained by ellipsometry from a polished[4] dense layer was in good agreement with the one derived with the RefDex software for an unpolished dense layer, validating our approach.

3.2.1. Film density

In order to determine the void fraction we used a technique based on EDX. The technique relies on the relationship between electron beam energy, interaction volume and material density, and was empirically found by Kanaya and Okayama [29]. The interaction volume of a porous layer depends on its thickness and density, since the voids inside a material do not absorb electrons. Electrons that have to cross a thick and dense film will need a larger energy compared to those going through a thin and porous layer. The corresponding energy is

[4] The ZnO dense layer was polished by mechanical brushing its surface in a solution of nanosilica particles (diameter around 40 nm).

Table 1. Minimal EDX energy, film thickness, relative density and void fraction for the dense (polished and as-deposited), flaked, and nanopillar films.

	E_0 keV	d μm	ρ_{rel} %	v_f %
Dense polished	13.6	0.65	100	0
Dense	19.0	1.17	97	3
Flaked	17.9	1.18	87	13
Nanopillars	14.9	0.99	76	24

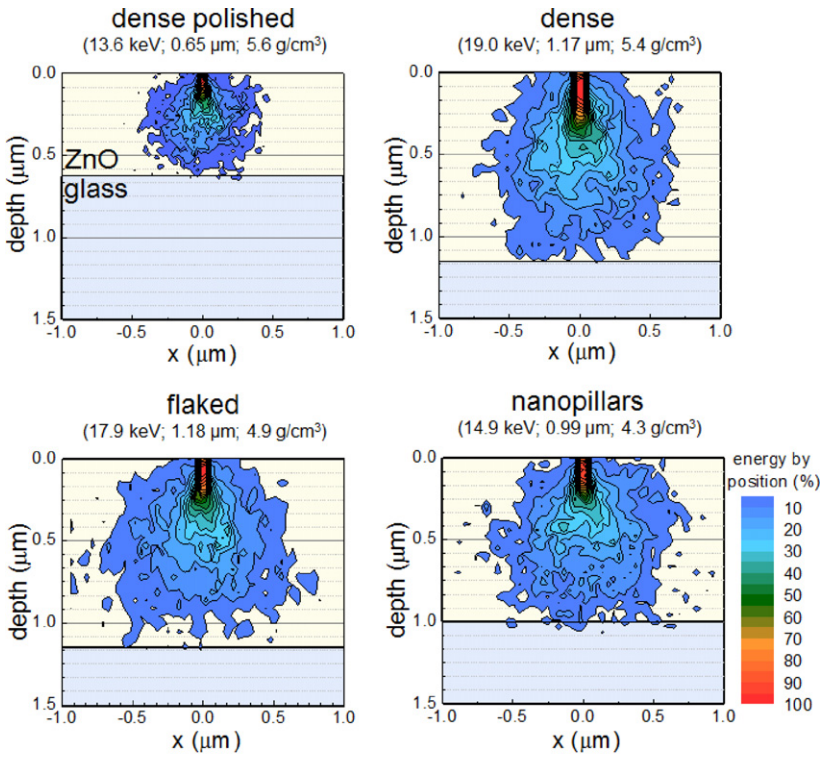

Figure 3. Simulated interaction volume between the EDX electron beam and ZnO film on glass for the four films analyzed. The different colored surfaces represent the energy of electrons with respect to the initial beam energy.

assessed by EDX as the minimal energy E_0 at which it is possible to observe the x-ray signal coming from elements characteristic of the glass substrate. Knowing the thickness, and supposing that electrons are absorbed exclusively by ZnO (atomic number $Z_{ZnO} = 38$, and atomic mass $A_{ZnO} = 81.4$) the density (ρ, in arbitrary units) of the inhomogeneous film can be found according to [29]:

$$\rho = \frac{2.76 \times 10^{-2} \cdot A \cdot E_0^{1.67}}{d \cdot Z^{0.89}}. \quad (2)$$

Assuming that the polished dense ZnO film is fully compact ($v_f = 0$) it is useful to define the relative film density as $\rho_{rel} = \rho/\rho_{dense\_ZnO}$. Thus, the void fraction for the other layers can be given by $v_f = 1 - \rho_{rel}$. With this procedure, we estimate a void fraction of up to 24% for the film characterized by nanopillars, as shown in table 1.

As defined above, E_0 is the minimal beam energy allowing a certain share of the incoming electrons to pass through the ZnO layer and to release from the glass constituents enough x-rays to be detected. In order to verify the results obtained with equation (2), we simulated the interaction volume of the electron beam with the ZnO films using the software CASINO [30]. Each simulation was characterized by means of the measured values of E_0, d and ρ_{rel} listed in table 1 and using 5.6 g cm^{-3} for ρ_{dense_ZnO}. Figure 3 shows the energy of the electrons with respect to their position in the film. Note that the average energy of the electrons reaching the glass is close to 5% of the initial beam energy for all four samples, even though they have a unique value of E_0, d, and ρ_{rel}. The fact that the beam energy at the ZnO/glass interface is very close in all four cases is consistent with the measurements.

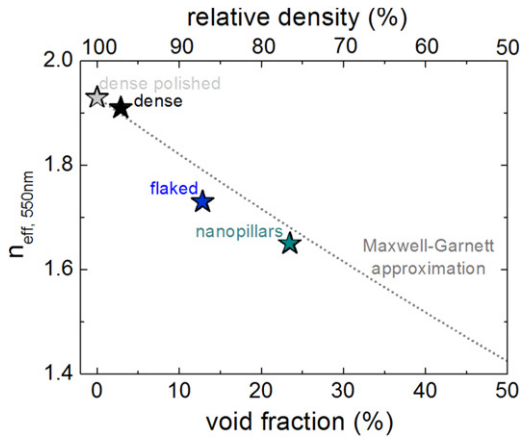

Figure 4. Effective refractive index (at 550 nm) versus relative density for the polished dense, dense, flaked and nanopillar films. Measured (stars, table 1) and simulated (dotted line, equation (1)) results are compared.

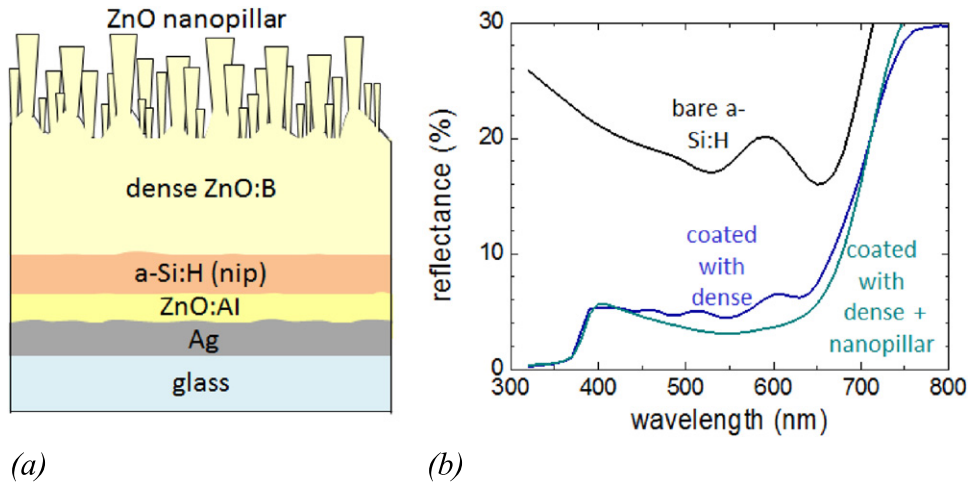

Figure 5. (a) Schematic, not in scale, of the nip cells showing the lowest reflectance: the front electrode is composed by an upper ZnO nanopillar layer (antireflective) and a lower ZnO dense layer (providing lateral conductivity). (b) Reflectance of different a-Si:H cells: not coated, coated with a dense film, and with a dense film + nanopillar film (as sketched in figure 5(a)).

3.2.2. Film density and effective refractive index

Table 1 shows how the void fraction increases during the transition from a dense film to a nanopillar film; moreover the relation of the film void fraction to n_{eff} (figure 2(b)) is found to be linear as shown in figure 4 (stars). This dependence is in good agreement with equation (1) which predicts n_{eff} based on void fraction (figure 4, gray dashed line). This confirms the applicability of the effective-medium theory approach in estimating the refractive index of the highly porous nanopillar films.

3.3. Application in a-Si:H solar cells

In an a-Si:H cell in the n–i–p configuration, a top layer consisting of a transparent conductive oxide acts as the front electrode (figure 5). Dense LP-MOCVD ZnO films are proven excellent electrodes for this purpose with a sheet resistance around 10 Ω_{sq} and absorptance below 5% in the visible range [31]. In order to have both, the excellent optoelectronics properties of the LPCVD ZnO and the antireflective properties of the nanopillar layer, we have combined both on a sequential deposition as presented in figure 5.

This approach is commonly applied in optoelectronic devices [31, 32]. Moreover a layer composed of nanoparticles (having a low refractive index) has been successfully applied as an intermediate reflector layer between the top and the bottom cell in tandem solar cells [33, 34]. Figure 5 shows that when the a-Si:H is coated with the dense ZnO film, the reflectance of the solar cell decreases from 20 to 6% in the spectral range between 400 and 650 nm. When the ZnO nanopillar film is deposited on top of the front ZnO contact (dense film), the reflectance is further decreased. This is a result of the graded transition introduced by the nanopillar film

Table 2. Sheet resistance for dense, flaked, nanopillars and nanopillars on dense films.

	Non intentionally doped		doped	
	d (μm)	R_{sh} (Ω_{sq})	d (μm)	R_{sh} (Ω_{sq})
Dense	1.17	1.8×10^2	0.97	22
Flaked	1.18	3.2×10^2	1.05	2.9×10^2
Nanopillars	0.99	6.1×10^6	1.03	5.3×10^6
Dense + Nanopillars	1.17 + 0.99	2.3×10^2	0.97 + 1.03 (nid)	39

between the refractive index of air and that of dense ZnO. The cell coated with dense ZnO + ZnO nanopillar layer has a reflectance close to 4% in the 400–650 nm spectral range.

The porosity of the ZnO nanopillar layer reduces the carrier lateral mobility, which dramatically increases the film sheet resistance. However, the combination of nid ZnO nanopillars on top of the dense B-doped ZnO provides the low sheet resistance (39 Ω_{sq} for doped ZnO) required for application as an electrode in solar cells. It should be noticed that the addition of boron in the dense film changes its optical properties mainly in the ultraviolet ($\lambda < 400$ nm, Burstein–Moss effect) and in the infrared regions ($\lambda > 1000$ nm, free carrier absorption) as often reported in literature [12, 13]. Therefore within the range of the spectral response of a-Si:H, the optical properties of the dense doped film are very similar to the one of the nid film discussed in the previous sections. Table 2 presents a summary of the electrical properties of the layers.

4. Conclusions

We showed how the void fraction of ZnO thin films can be easily and finely tuned by adjusting the substrate temperature and the ratio of precursor gases during the LP-MOCVD process. Three ZnO films characterized by a decreasing compactness were deposited and their bulk void fraction was quantified by means of EDX measurements. The film characterized by nano-sized pillars showed the highest void fraction of 24%; for these films, the effective refractive index, derived by optical measurements, was assessed to be $n = 1.65$. The compactness decrease leads to a refractive index decrease in agreement the effective-medium theory. Finally due its high transmittance and low reflectance the nanopillar are exploited as antireflective layer on top of the front contact of an amorphous silicon solar cell, reducing its reflectance to around 4% in the visible range.

Acknowledgments

The authors thank Dr A Hessler-Wysler for helpful discussions regarding EDX measurements, P Manley (Helmholtz Zentrum Berlin) for the advice in the use of the RefDex software, L Sands for carefully reviewing the manuscript. This work was funded by the Swiss National Science Foundation (FNS) under the project ZONEM (no. 513258).

References

[1] Wan Q, Li Q H, Chen Y J, Wang T H, He X L, Li J P and Lin C L 2004 *Appl. Phys. Lett.* **84** 3654
[2] Jing Z and Zhan J 2008 *Adv. Mater.* **20** 4547
[3] Li J, Fan H and Jia X 2010 *Phys. Chem.* C **114** 14684
[4] Mei A *et al* 2014 *Science* **34** 295
[5] Noel N K *et al* 2014 *Energy Environ. Sci.* **7** 3061
[6] Nicolay S, Despeisse M, Haug F J and Ballif C 2011 *Sol. Energy Mater. Sol. Cells* **95** 1031
[7] Prasad A, Balakrishnan S, Jain S K and Jain G C 1982 *J. Electrochem. Soc.* **129** 596
[8] Schirone L, Sotgiu G and Califano F P 1997 *Thin Solid Films* **297** 296
[9] Chen J, Wang B, Yang Y, Shi Y, Xu G and Cui P 2012 *Appl. Opt.* **51** 683
[10] Kennedy S R and Brett M J 2003 *Appl. Opt.* **42** 4573
[11] Potter R R 1986 *Sol. Cells* **16** 521
[12] Faÿ S, Kroll U, Bucher C, Vallat-Sauvain E and Shah A 2005 *Sol. Energy Mater. Sol. Cells* **86** 385
[13] Wenas W W, Yamada A, Takahashi K, Yoshino M and Konagai M 1991 *J. Appl. Phys.* **70** 7119
[14] Nicolay S, Benkhaira M, Ding L, Escarre J, Bugnon G, Meillaud F and Ballif C 2012 *Sol. Energy Mater. Sol. Cells* **105** 46
[15] Steele J J and Brett M J 2007 *J Mater. Sci: Mater. Electron* **18** 367
[16] Robbie K, Sit J C and Brett M J 1997 *J. Vac. Sci. Technol.* **B13** 1115
[17] Morales-Masis M, Segura L and Ramírez-Porras A 2007 *Appl. Surf. Sci.* **253** 7188
[18] Fanni L, Aebersold B A, Alexander D T L, Ding L, Morales Masis M, Nicolay S and Ballif C 2014 *Thin Solid Films* **565** 1
[19] Biron R *et al* 2013 *Sol. Energy Mater. Sol. Cells* **114** 147
[20] Manley P, Yin G and Schmid M 2014 *J. Phys. D: Appl. Phys.* **47** 205301
[21] (www.b-nano.com)

[22] Nicolay S, Fay S and Ballif C 2009 *Cryst. Growth Des.* **9** 4957
[23] Maejima K, Koida T, Sai H, Matsui T, Saito K, Kondo M and Takagawa T 2014 *Thin Solid Films* **559** 83
[24] Faÿ S 2003 *PhD Thesis* EPFL
[25] Choy T C 1999 *Effective Medium Theory: Principles and Applications* (New York: Oxford University Press)
[26] Levy Y, Jurich M and Swaien J D 1985 *J. Appl. Phys.* **57** 2601
[27] Yoldas B E and Partlow D P 1985 *Thin Solid Films* **129** l
[28] Kumar Raut H, Ganesh V A, Nairb A S and Ramakrishna S 2011 *Energy Environ. Sci.* **4** 3779
[29] Kanaya K and Okayama S 1972 *J. Phys. D: Appl. Phys.* **5** 43
[30] Drouin D, Réal Couture A, Joly D, Tastet X, Aimez V and Gauvin R 2007 *Scanning* **29** 92
[31] Ding L, Boccard M, Bugnon G, Benkhaira M, Nicolay S, Despeisse M, Meillaud F and Ballif C 2012 *Sol. Energy Mater. Sol. Cells* **98** 331
[32] Welser R E, Sood A W, Cho J, Schubert E F, Harvey J L, Dhar N K and Sood A K 2012 *MRS Fall Meeting* vol 1493
[33] Kim J K, Gessmann T, Schubert E F, Xi J-Q, Luo H, Cho J, Sone C and Park Y 2006 *Appl. Phys. Lett.* **88** 013501
[34] Niesen B, Blondiaux N, Boccard M, Stuckelberger M, Pugin R, Scolan E, Meillaud F, Haug F-J, Hessler-Wyser A and Ballif C 2014 *Nano Lett.* **14** 5085